Intrinsic optoelectronic characteristics in MoS_2 phototransistors via a fully transparent van der Waals heterostructure

Jinsu Pak[1], Ilmin Lee[2], Kyungjune Cho[1], Jae-Keun Kim[1], Hyunhak Jeong[1,†], Wang-Taek Hwang[1], Geun Ho Ahn[3,†], Keehoon Kang[1], Woo Jong Yu[2], Ali Javey[3], Seungjun Chung[4] & Takhee Lee[1]

[1]Department of Physics and Astronomy, and Institute of Applied Physics, Seoul National University, Seoul 08826, Korea

[2]Department of Electrical and Computer Engineering, Sungkyunkwan University, Suwon 16419, Korea

[3]Electrical Engineering and Computer Sciences, University of California, Berkeley, California 94720, USA

[4]Photoelectronic Hybrids Research Center, Korea Institute of Science and Technology (KIST), Seoul 02792, Korea

[†]Current addresses: Department of Electrical and Computer Engineering, University of California, Davis, California 95616-5270, USA (H. J.); Department of Electrical Engineering, Stanford University, Stanford, California 94305, USA (G. H. A.)

Seungjun Chung and Takhee Lee jointly supervised this work. Correspondence and requests for materials should be addressed to S. C. (e-mail: seungjun@kist.re.kr) or to T. L. (e-mail: tlee@snu.ac.kr).

KEYWORDS: MoS_2, phototransistor, heterostructure, internal quantum efficiency, internal responsivity

ABSTRACT

Recently, optoelectronic studies of MoS_2-based phototransistors have been carried out for achieving high performance. However, the intrinsic optoelectronic characteristics in MoS_2 remain unexplored because of unintended interferences originating from commonly used opaque substrates such as SiO_2/Si, which lead to overestimated photoresponsive characteristics due to enhanced photogating and photoconductive effects. Here, we investigated the intrinsic photoresponsive characteristics, including internal responsivity and quantum efficiency, in fully transparent monolayer MoS_2 phototransistors employing a van der Waals heterostructure. As opposed to previous reports, the internal photoresponsive characteristics do not significantly depend on the wavelength of the incident light as long as the electron-hole pairs are generated in the same *k*-space. This study provides a deeper understanding of the photoresponsive characteristics in MoS_2 and lays the foundation for two-dimensional materials-based transparent phototransistors.

Beginning with extensive research on graphene, the emergence of a new class of atomically thin two-dimensional (2D) materials has opened up a new era for fundamental scientific studies and the next generation of electronics[1–3]. In this group of 2D materials, especially molybdenum disulfide (MoS_2) has been extensively studied as a promising candidate for realizing 2D materials-based flexible photodetectors due to its outstanding optoelectronic properties, such as intrinsic bandgap, high photodetection capability, high carrier mobility, good electrical stability, and mechanical flexibility[4–7]. Recently, MoS_2-based 2D heterostructures have been designed to enhance photodetection and photoswitching abilities, which is attributed to the high-quality interfacial properties present between 2D materials held together by the weak van der Waals (vdW) interaction without covalent bonds. For instance, vdW heterostructured MoS_2 photodiodes made with tungsten diselenide (WSe_2), molybdenum ditelluride ($MoTe_2$), and black phosphorus have been realized to improve photoresponsive characteristics[8–12]. Also, MoS_2 phototransistors with hexagonal boron nitride (*h*-BN), graphene, and tin diselenide ($SnSe_2$) in a vertical vdW heterostructure have shown enhanced responsivity or faster photoswitching behavior[13–15]. Although numerous studies of the optical properties of vdW heterostructured photodetectors have been reported, to date, the intrinsic optical characteristics of atomically thin MoS_2 have not been explored because most previous studies have employed opaque substrates, typically heavily-doped Si with SiO_2, due to the convenience from a manufacturing perspective. The opaque platforms allow

multiple reflections of incident light, which results in the generation of additional electron-hole pairs at the MoS_2/SiO_2 and SiO_2/Si[16] interfaces. Furthermore, this unintended interference causes a strong photogating effect due to the trapping of photogenerated holes at the poor interface[17,18], which can overestimate the ability of the photoresponsivity of MoS_2. For a better understanding of MoS_2, in this regard, the study of the intrinsic optoelectronic characteristics of MoS_2 without effects caused by external interference such as reflected or refractive light is highly desirable.

Here, we investigated the intrinsic optoelectronic characteristics of monolayer MoS_2 phototransistors via a fully transparent vdW heterostructure with *h*-BN (as a dielectric layer) and graphene (as a gate electrode). The 2D *h*-BN dielectric provided a near-ideal interface with MoS_2 enabling low-voltage operation. To investigate the intrinsic photoresponsive properties of MoS_2, we compared the characteristics of the MoS_2 phototransistors fabricated on transparent polyethylene naphthalate (PEN) and opaque SiO_2/Si substrates. From the results, it turned out that the MoS_2 phototransistor fabricated on the opaque SiO_2/Si substrate showed a higher photoresponsive performance due to enhanced photogating and photoconductive effects caused by the opaque substrate. The MoS_2 phototransistor fabricated on the transparent PEN substrate revealed intrinsic photoresponsive properties; specifically, an internal responsivity of 3.2×10^2 A/W and internal quantum efficiency (IQE) of 7.1×10^5 % were achieved. Interestingly, unlike the external photoresponse determined by the

incident photons that shows highly wavelength-dependent characteristics, the internal photoresponse determined by absorbed photons in the MoS_2 channel did not significantly depend on the wavelength of the incident light. Furthermore, it was observed that the intrinsic photoresponsive characteristics of MoS_2 could be dependent on the locations where photogeneration occurred in *k*-space and the consequent alteration of the effective mass.

Results

Structure and electrical characteristics of transparent MoS_2 phototransistors.

To realize transparent MoS_2 phototransistors, ready-made MoS_2 field-effect transistors (FETs) on a SiO_2/Si substrate were transferred to a PEN substrate via the transfer method using potassium hydroxide etching solution (see Methods and Supplementary Figure S1 for more details of the fabrication process). To produce reliable MoS_2 phototransistors, chemical vapor deposition (CVD)-grown monolayer MoS_2 was used as a channel layer in 2D vdW heterostructured FETs. In addition, by employing CVD-grown monolayer graphene as a gate electrode and mechanically exfoliated multilayer *h*-BN (41-nm thick) as a gate dielectric on a transparent PEN substrate (125-μm thick), good transparency of over 80 % in the visible range was achieved. Figure 1a shows a schematic illustrating the vertically stacked vdW heterostructure on a PEN substrate. After the realization of the 2D heterostructure using a micro-manipulator system (AP-4200GP, UNITEK), no drastically degraded transparency was observed in the optical image (Figure 1b). Raman frequency difference (20 cm^{-1}) (upper panel, Figure 1c) and a photoluminescence (PL) mapping image displaying uniform bandgap energy (1.86 eV) (Figure 1d) support the fact that the CVD-grown MoS_2 used for the channel was a uniform monolayer[19]. In addition, the Raman peak observed for the multilayer *h*-BN at 1364 cm^{-1} is assigned to the in-plane vibration (E_{2g} mode)[20]. The large intensity of the 2D-band relative to the G-band, which can

only be observed in monolayer graphene due to a triple-resonance process, shows that monolayer graphene film was well grown via the optimized CVD process (lower panel, Figure 1c)[21]. All Raman spectra in Figure 1c were measured before transfer to a PEN substrate for observing the distinct spectrum.

Figures 1e and 1f show the transfer curve (drain-source current versus gate voltage, I_{DS}-V_{GS}) and the output curve (drain-source current versus drain voltage, I_{DS}-V_{DS}) for the transparent CVD-grown monolayer MoS_2 FET measured in vacuum (~10^{-4} Torr) at room temperature. Arising from the thin *h*-BN dielectric layer, a low operation voltage ranging from -4 V to 5 V was achieved. The field-effect mobility (μ) was determined to be 12.2 cm^2/V•s, as calculated using the formula

$$\mu = \left(\frac{\partial I_{DS}}{\partial V_{GS}} \right) \frac{L}{W} \frac{1}{C_i V_{DS}}, \qquad (1)$$

with a channel width W = 8.56 μm, channel length L = 5.05 μm, and unit capacitance for the *h*-BN dielectric C_i = 0.756 mF/cm^2 (thickness of 41 nm and dielectric constant of 3.5 for *h*-BN were considered[22,23]). Figure 1g shows the logarithmic scale plot for I_{DS}-V_{DS} measured at V_{GS} ranging from 0 V to 5 V. The extracted average γ (linearity parameter in the output curve) value of 1.01 indicates ohmic contacts between the MoS_2 channel layer and Au electrodes.

Spectroscopic characteristics of the transparent MoS_2 phototransistors. Figure 2a shows the transmittance and reflectance of various stacks of individual layers; transparent substrate (PEN), CVD-grown monolayer graphene (denoted as Gr)/PEN, *h*-BN/Gr/PEN, and CVD-grown monolayer MoS_2/*h*-BN/Gr/PEN. Negligible absorption in the visible range for Gr and multilayer *h*-BN were verified through the observation of unchanged transmittance values after stacking Gr and *h*-BN onto a PEN substrate. The absorbance of CVD-grown monolayer MoS_2 was determined by subtracting the reflectance of the MoS_2 layer from the diminished transmittance after stacking the MoS_2 layer onto an underlying *h*-BN/Gr/PEN layer (Figure 2b). The extracted absorbance of the MoS_2 layer was used as a reference to investigate the internal optoelectronic characteristics which indicate the optoelectronic characteristics due to absorbed photons, not due to incident photons, in the MoS_2 phototransistor. In Figure 2b, the resonance peaks A and B correspond to excitonic transitions split by spin-orbit coupling at the K point in *k*-space[19]. The strong resonance peak C is ascribed to the parallel bands in the density of states even for excitation energy far exceeding the bandgap of MoS_2; this is called the band-nesting effect, which leads to a divergence in the joint density of states[24,25]. By employing transparent layers of Gr, MoS_2, *h*-BN, and PEN, fully transparent MoS_2 phototransistors were implemented with high transparency, as shown in Figure 2c. Also, laser-light fully penetrated through the transparent MoS_2 phototransistors without reflection or dispersion (right, Figure 2c).

Comparison of the optoelectronic characteristics of MoS_2 phototransistors on transparent and opaque substrates. To investigate the effects of the unintended photoresponsive characteristics, which are due to the use of an opaque substrate, CVD-grown monolayer MoS_2 phototransistors were fabricated with a *h*-BN dielectric on both a transparent PEN substrate (MoS_2/*h*-BN/Gr, denoted as MhG) and an opaque 100-nm-thick SiO_2/Si substrate (MoS_2/*h*-BN/heavily-doped silicon, denoted as MhS), as depicted in Figures 3a and 3b, respectively. The photoresponsive characteristics for MhG and MhS were investigated under various illumination conditions with different light intensities ranging from 15 nW to 1180 nW at a fixed wavelength of 450 nm and with different wavelengths ranging from 780 nm to 450 nm at a fixed light intensity of 3 μW in ambient air at room temperature (Figures 3c-3f). Note that the laser spot size was ~1 μm, which is smaller than the channel area dimension, so that the entire laser-light was focused within the MoS_2 channel area. As shown in Figures 3c-3f, the photoinduced current steadily increased in both types of devices, MhG and MhS, as the illumination intensity became stronger at a fixed wavelength (Figures 3c and 3e) and also as the wavelength of the incident light became shorter at a fixed illumination intensity (Figures 3d and 3f). As shown in Figures 3d and 3f, the electron-hole pairs could be created by illumination with a laser photon energy (1.59 eV and 1.80 eV, corresponding to 780 nm and 688 nm, respectively) smaller than the optical bandgap energy of MoS_2

(1.9 eV)[26] via the excitation of carriers localized in band tail states. For a more accurate comparison, the gate electric field (E_{GS}) instead of V_{GS} was used as the x-axis in Figures 3c-3f because of the different thicknesses of the dielectric layers in MhG and MhS. There were two noticeable distinctions in the photoresponsive characteristics for MhG and MhS: 1) the amount of change in the threshold electric field (ΔE_{TH}) in MhS due to illumination was larger than that in MhG (Figure 3g), and 2) the responsivity (R) of MhS was higher than that of MhG (Figure 3h). To understand the difference in the photoresponsive properties between MhG and MhS, the components of the photoinduced current should be classified.

To date, various mechanisms for the photoinduced current in MoS_2 have been proposed, such as the photoelectric (PE), photothermoelectric (PTE), photogating (PG), and photoconductive (PC) effects. Typically, the PE and PTE effects dominate in the photoresponse in cases without an electric field; therefore, the PG and PC effects dominantly determine the photoconductivity in phototransistors when an electric field is applied[17]. The PG effect is attributed to structural defects in MoS_2 itself or to disorder caused by the imperfect interface with the substrate at which the photogenerated electrons or holes can be trapped, playing the role of a local gate electric field. In *n*-type MoS_2-based FETs, a negative shift in the threshold voltage (V_{TH}) is typically observed due to the PG effect via the trapped photogenerated holes[17]. In contrast, the PC effect corresponds to the contribution of

increased channel current due to the photogenerated carriers in the channel, which influence V_{TH} less. So, the total photocurrent (I_{ph}) can be expressed as

$$I_{Ph}=I_{Ph,PG}+I_{Ph,PC}=g_m\left|\Delta V_{TH}\right|+\left(\frac{W}{L}\right)V_{DS}\Delta\sigma, \qquad (2)$$

where $g_m=\frac{dI_{DS}}{dV_{GS}}$ is the transconductance and $\Delta\sigma=q\mu_n\Delta n$ is the change in conductivity due to the photogenerated carriers. Although the proportion between the PG and PC effects differs depending on the device structure, typically, the PG effect is more dominant in vdW materials[17]. If photogenerated minority carriers are trapped with a certain spatial distribution, their lifetime becomes prolonged; therefore, this can produce an additional gate electric field until they disappear through recombination[27,28]. When the majority carriers pass through the channel for contributing to the photocurrent, additional majority carriers should be injected into the channel to preserve charge neutrality until the trapped photogenerated holes disappear[27,28]. Therefore, the photoresponsive characteristics in vdW materials-based phototransistors can be amplified by trapping photogenerated minority carriers as well as by applied electric fields for accelerating the movement of the majority carriers.

In this regard, the higher value of $\left|\Delta E_{TH}\right|$ for MhS in the low illumination intensity regime than that for MhG (blue area in Figure 3g) indicates that the PG effect in MhS was stronger than that in MhG in the low illumination intensity regime. This behavior is due to the influence of the reflected light from the SiO_2/Si substrate along with the PG effect. In our study, the PG

effect arises dominantly from the trapped holes at the intrinsic defects such as sulfur vacancies in MoS_2[29], but not at the interface trap sites because the underlying inserted *h*-BN layer provided a near-ideal interface with MoS_2. Therefore, the reflected light from the SiO_2/Si substrate in MhS can generate more trapped photogenerated holes, which leads to the enhanced PG effect in MhS in the low illumination intensity regime. However, in the high illumination intensity regime, most trap sites can be occupied by sufficient photogenerated holes in both MhS and MhG. Thus, the values for $|\Delta E_{TH}|$ for MhS and MhG became comparable in the high illumination intensity regime (red area in Figure 3g).

Figure 3h shows the responsivity for MhS and MhG as a function of wavelength measured at a fixed V_{DS} of 0.5 V, E_{GS} of 0 MV/cm, and illumination intensity (P) of 3 μW. Note that the maximum power for the illumination intensity was restricted up to 3 μW to prevent any undesirable physical damage to the atomically thin monolayer MoS_2 channel. The responsivity (R) is an important parameter for evaluating the performance for photodetector applications, which is defined as

$$R = \frac{I_{Ph}}{P_{Light}}, \qquad (3)$$

where P_{Light} is the illumination intensity. We observed a higher responsivity for MhS than that for MhG under various wavelengths ranging from 780 nm to 450 nm at a fixed intensity of 3 μW, as shown in Figure 3h. This result is also attributed to the light reflected from the SiO_2/Si substrate along with the

PC effect. Because the PG effects in MhS and MhG are comparable under high intensity illumination, the reason for the higher responsivity of MhS is attributed to the stronger PC effect in MhS, which originates from additional carrier creation by the reflected light from the SiO_2/Si substrate (Figure 3h). In addition, the responsivity under the various illumination intensities ranging from 15 nW to 1180 nW at a fixed wavelength of 450 nm is indicated in the inset of Figure 3h. Due to the stronger PG effect in MhS in the low illumination intensity regime, a much higher responsivity was observed in MhS than in MhG; then, the responsivity values became comparable between MhS and MhG as the illumination intensity was increased (inset of Figure 3h). As the illumination intensity increased, the responsivity of MhS was reduced, whereas a nearly constant responsivity was observed for MhG. The decline of the responsivity for increasing illumination intensity for MhS can be explained in terms of restricted trap sites. In the low illumination intensity regime, a substantial portion of the photogenerated holes can be trapped and act as a positive gate electric field, leading to increased responsivity. On the other hand, in the high illumination intensity regime, the possibility for trapping becomes lower due to a sufficient number of photogenerated holes being more than the number of trap sites, which results in reduced responsivity (inset of Figure 3h). Similar phenomena have been reported in MoS_2 phototransistors[30,31]. Therefore, the photoresponsive characteristics in MoS_2 phototransistors fabricated on opaque substrates are overestimated,

which cannot be regarded as the intrinsic optoelectronic characteristics of MoS_2.

Intrinsic optoelectronic characteristics of the transparent MoS_2 phototransistor under visible light. To explore the intrinsic optoelectronic properties of MoS_2, the dependencies of the optoelectronic characteristics of transparent MhG on V_{GS} and wavelength were investigated (Figure 4). Note that the intrinsic optoelectronic results under the various illumination intensities are provided in Supplementary Figures S3-S5. The contour plots indicating external and internal responsivities as a function of V_{GS} and wavelength measured at a V_{DS} of 0.5 V are displayed in Figure 4a. Because the internal and external responsivity values are defined as the photocurrent per watt of the absorbed and incident illumination intensity, respectively, the internal responsivity is calculated by dividing the external responsivity by the absorbance of the MoS_2 layer (Figure 2b). In other words, the values for the internal responsivity are higher than those for the external responsivity under the entire range of wavelengths (Figure 4a). To achieve the maximum responsivity in phototransistors, low illumination intensity, high V_{DS}, and high V_{GS} are required (for details, see Supplementary Figure S3). Under optimum measurement conditions, a maximum external responsivity of 16.8 A/W and maximum internal responsivity of 3.2×10^2 A/W were achieved (Supplementary Figure S6). Figure 4c exhibits contour plots comparing the external quantum efficiency (EQE) and internal quantum

efficiency (IQE) versus V_{GS} and wavelength for a transparent MoS_2 phototransistor measured at V_{DS} of 0.5 V and illumination intensity of 3 μW. EQE and IQE are defined as the number of carriers detected per incident photon and absorbed photon, respectively, as defined by the following formula:

$$EQE(\%)=\frac{I_{Ph}/e}{P_{Inc}/hv}\times 100 \quad \text{and} \quad IQE(\%)=\frac{I_{Ph}/e}{P_{|¿|}/hv\times 100¿}, \qquad (4)$$

where P_{Inc}, $P_{|¿|¿}$, and hv are the incident illumination intensity, absorbed illumination intensity, and photon energy, respectively. Similar to the dependency of the responsivity on V_{GS} (Figure 4b), EQE and IQE also increased with increasing V_{GS} at a fixed V_{DS} of 0.5 V (Figure 4c). For an in-depth understanding of the quantum efficiency dependence on the wavelength of the light, the EQE values extracted from the contour plot of Figure 4c are exhibited in Figure 4d. Note that the condition of $V_{GS} > V_{TH}$ ranging from 2 V to 5 V was taken into account in Figures 4d and 4e in which photogenerated carriers can contribute to the photocurrent efficiently. An abrupt increase in EQE was observed at a wavelength of around 620 nm due to the A- and B-excitonic transitions represented as the resonance peaks in the absorbance of MoS_2 (red line curve in Figure 4d). Higher EQE was also observed near the strong resonance peak at ~440 nm corresponding to the C-excitonic transition induced by the band-nesting effect[24,25].

In contrast, the IQE values by the C-excitonic transition were lower than those by the A- or B-excitonic transition, as shown in Figure 4e. Previous

studies of the C-excitonic transition in MoS_2 reported that the photogenerated electrons and holes in the band-nesting region are well separated in *k*-space to their immediate band extremum[25,32]. Because the photogenerated electrons and holes in the band-nesting region move quickly to the Λ valley and Γ hill[24,25,32], respectively, on an extremely fast intraband relaxation time scale of C-exciton (< 500 fs)[33], a more enhanced photodetection ability could be expected under the C-excitonic transition due to the suppression of direct band-to-band recombination[32]. However, contrary to this anticipation, the photogenerated carriers excited by the A- or B-excitonic transition produced a higher IQE than that produced by the C-excitonic transition (Figure 4e). Note that a similar consequence was observed in the internal responsivity (see Supplementary Figure S7). These phenomena can be explained by the different effective masses of the carriers located at different positions in *k*-space. For the photodetection ability in *n*-type MoS_2 phototransistors, the effective mass of the electron is typically a more significant parameter because majority carriers (electrons) are accelerated by applied electric fields, thus contributing to the photocurrent, while minority carriers (holes) are trapped with a long lifetime. However, regardless of the types of carriers, the effective mass of the electron (hole) located at the Λ valley (Γ hill) created by the C-excitonic transition is heavier than that created by the A- or B-excitonic transitions at the K point[34,35]. In this manner, although the electron-hole pairs photogenerated by the C-excitonic transition can be easily separated without

extinction by recombination, the IQE values under illumination at 450 nm (C-excitonic transitions) were 58% of those under illumination at 600 nm (B-excitonic transition), as extracted from the results measured at V_{GS} from 2 V to 5 V (Figure 4e). Interestingly, in contrast to the EQE and external responsivity, the IQE and internal responsivity did not exhibit a significant dependence on the wavelength of visible light. In addition, the IQE can also be amplified up to 7.1 × 10^5 % by the applied electric fields (V_{GS} and V_{DS}) under low illumination intensity (Supplementary Figure S6).

Time-resolved photoresponse characteristics in the transparent MoS_2 phototransistor. We investigated the temporal evolution of the photoresponse of MhG measured at a V_{DS} of 1.0 V and 0.1 V and at a fixed V_{GS} of –2 V (illuminated by a laser with a wavelength of 620 nm and an intensity of 20 nW), as shown in Figure 5a. After illuminating the MoS_2 channel for 100 s, the decay process for the photoinduced current was examined after turning the laser off. The decay process followed an exponential decay function with two different decay constants (τ_1 and τ_2) according to the time range[36]. Even though high-quality MoS_2 phototransistors with a vdW heterostructure were realized, a long-lasting photoconductivity was inevitably observed after turning the laser off [13,17,30] (Figure 5). The origin for the long-lasting photoconductivity in the decay has been described as being due to the influence of random local potential fluctuations (RLPF) in the band structure[37,38] and influence of the trapped

photogenerated minority carriers that hinder recombination in the forbidden gap of MoS_2[13,27–29]. The confined carriers can escape the potential even after the laser is turned off and then contribute to the photocurrent, resulting in a long decay time. In addition, the trapped photogenerated holes in MoS_2 consistently induce the injection of electrons for charge neutrality until they disappear through the recombination process. In this regard, the increase in V_{DS} from 0.1 V to 1.0 V promoted the release of confined carriers in RLPF and reduced the lifetime of the trapped photogenerated holes, so the τ_1 (τ_2) value decreased from 66.8 s (86.5 s) to 14.0 s (56.3 s), as shown in Figures 5a and 5b. Figure 5c shows the time-resolved photoresponse under illumination with different intensities of 1150 nW and 40 nW measured at a fixed V_{GS} of –2 V and V_{DS} of 1 V (illuminated by a laser with a wavelength of 620 nm). Because the high illumination intensity created more photogenerated electron-hole pairs, which leads to increased carrier confinement in RLPF or in the trap sites in the forbidden gap, the τ_1 (τ_2) value increased from 20.2 s (53.8 s) to 24.9 s (60.9 s) as the illumination intensity was increased from 40 nW to 1150 nW (Figure 5d). Also, the time-resolved photoresponse was not significantly affected by the wavelength of the laser because different photon energies cannot change the lifetime of the photogenerated holes trapped in the forbidden gap of MoS_2 (Supplementary Figure S8).

Discussion

This work explores, for the first time, the internal optoelectronic characteristics in fully transparent MoS_2 phototransistors by employing a 2D

vdW heterostructure. From the systematic comparison of the optoelectronic characteristics between transparent and opaque MoS_2 phototransistors, it turns out that the photoresponsive characteristics of MoS_2 are overestimated due to enhanced photogating and photoconductive effects originating from the use of opaque substrates. In addition, we found that a maximum internal responsivity of 3.2×10^2 A/W and IQE of 7.1×10^5 % were yielded in a fully transparent MoS_2 phototransistor, which can be regarded as the intrinsic optoelectronic characteristics of CVD-grown monolayer MoS_2. Interestingly, in contrast with the external photoresponse, which was highly wavelength-dependent, the internal photoresponse did not significantly depend on the wavelength of the incident light. Furthermore, relatively lower IQE values at the C-excitonic transitions than those at the A- or B-excitonic transition show different optoelectronic properties depending on the locations of the photogenerated carriers in *k*-space due to their different effective masses. Our study helps in understanding the intrinsic optoelectronic characteristics of CVD-grown monolayer MoS_2, and it will provide insight into the realization of 2D materials-based transparent optoelectronics.

Methods

Fabrication of fully transparent MoS_2 FETs

To fabricate fully transparent MoS_2 FETs, large-area monolayer graphene grown on a copper foil by the CVD method was transferred onto a 270-nm-thick SiO_2/Si substrate. Next, a mechanically exfoliated multilayer *h*-BN was transferred onto the monolayer graphene by a micro-manipulator system (AP-4200GP, UNITEK). After transferring the CVD-grown monolayer MoS_2 onto the *h*-BN, the Au source and drain electrodes (30-nm thick) were formed through processes using electron beam lithography (JSM-6510, JEOL) and an electron beam evaporator (KVE-2004L, Korea Vacuum Tech.). For transfer onto a transparent substrate, the vdW heterostructured MoS_2 FETs coated with PMMA were immersed into a 50 % potassium hydroxide solution with annealing at 70 °C for etching the SiO_2/Si substrate. After that, the vdW heterostructure with the source and drain electrodes, which was held firmly by PMMA, was scooped up and transferred onto a 125-µm-thick PEN substrate. The fabricated transparent MoS_2 FETs were annealed at 80 °C in a vacuum for 2 h to eliminate residues on the surface of the MoS_2 channels.

Electrical and optical characterization

The electrical properties of the transparent MoS_2 FETs were measured using a semiconductor parameter analyzer (Keithley 4200-SCS) in vacuum. Transmittance and reflectance data for the vdW heterostructure were obtained by using a UV/Vis/NIR Microspectrometer (CRAIC, QDI-1000).

Raman spectra, PL spectra, and PL mapping of vdW materials were characterized using an XperRam 200 (Nanobase, Inc.) instrument using a 532 nm laser as the excitation source with a diffraction-limited laser spot size (~1 μm spot radius). In addition, an electroluminescence measurement system (Nanobase, Inc.) was used to investigate the optoelectronic characteristics of the transparent MoS_2 phototransistors.

References

1. Wang, Q. H., Kalantar-Zadeh, K., Kis, A., Coleman, J. N. & Strano, M. S. Electronics and optoelectronics of two-dimensional transition metal dichalcogenides. *Nat. Nanotechnol.* **7**, 699–712 (2012).

2. Manzeli, S., Ovchinnikov, D., Pasquier, D., Yazyev, O. V. & Kis, A. 2D transition metal dichalcogenides. *Nat. Rev. Mater.* **2**, 17033 (2017).

3. Mak, K. F. & Shan, J. Photonics and optoelectronics of 2D semiconductor transition metal dichalcogenides. *Nat. Photon.* **10**, 216–226 (2016).

4. Zhang, W., Huang, J.-K., Chen, C.-H., Chang, Y.-H., Cheng, Y.-J. & Li, L.-J. High-gain phototransistors based on a CVD MoS_2 monolayer. *Adv. Mater.* **25**, 3456–3461 (2013).

5. Yoon, Y., Ganapathi, K. & Salahuddin, S. How good can monolayer MoS_2 transistors be? *Nano Lett.* **11**, 3768–3773 (2011).

6. Yang, S., Park, S., Jang, S., Kim H. & Kwon, J.-Y. Electrical stability of multilayer MoS_2 field-effect transistor under negative bias stress at various temperatures. *Phys. Status Solidi RRL* **8**, 714–718 (2014).

7. Pu, J., Yomogida, Y., Liu, K.-K., Li, L.-J., Iwasa, Y. & Takenobu, T. Highly flexible MoS_2 thin-film transistors with ion gel dielectrics. *Nano Lett.* **12**, 4013–4017 (2012).

8. Furchi, M. M., Pospischil, A., Libisch, F., Burgdörfer, J. & Mueller, T. Photovoltaic effect in an electrically tunable van der Waals heterojunction. *Nano Lett*. **14**, 4785–4797 (2014).

9. Lee, C.-H. et al. Atomically thin p-n junctions with van der Waals heterointerfaces. *Nat. Nanotechnol.* **9**, 676–681 (2014).

10. Wang, F., Yin, L., Wang, Z. X., Xu, K., Wang, F. M., Shifa, T. A., Huang, Y., Jiang, C. & He, J. Configuration-dependent electrically tunable van der Waals heterostructures based on $MoTe_2/MoS_2$. *Adv. Funct. Mater.* **26**, 5499–5506 (2016).

11. Pezeshki, A., Shokouh, S. H. H., Nazari, T., Oh, K. & Im, S. Electric and photovoltaic behavior of a few-layer α-$MoTe_2/MoS_2$ dichalcogenide heterojuction. *Adv. Mater.* **28**, 3216–3222 (2016).

12. Ye, L., Li, H., Chen, Z. & Xu, J. Near-infrared photodetector based on MoS_2/black phosphorus heterojunction. *ACS Photonics* **3**, 692–699 (2016).

13. Tran, M. D., Kim, J.-H., Kim, H., Doan, M. H., Duong, D. L. & Lee, Y. H. Role of hole trap sites in MoS_2 for inconsistency in optical and electrical phenomena. *ACS Appl. Mater. Interfaces* **10**, 10580–10586 (2018).

14. Fazio, D. D. et al. High responsivity, large-area graphene/MoS_2 flexible photodetectors. *ACS Nano* **10**, 8252–8262 (2016).

15. Zhou, X. et al. Vertical heterostructures based on $SnSe_2/MoS_2$ for high performance photodetectors. *2D Mater.* **4**, 025048 (2017).

16. Lien, D.-H. et al. Engineering light outcoupling in 2D materials. *Nano Lett.* **15**, 1356–1361 (2015).

17. Furchi, M. M., Polyushkin, D. K., Pospischil, A. & Mueller, T. Mechanisms of photoconductivity in atomically thin MoS_2. *Nano Lett.* **14**, 6165–6170 (2014).

18. Huang, H. et al. Highly sensitive visible to infrared $MoTe_2$ photodetectors enhanced by the photogating effect. *Nanotechnology* **27**, 445201 (2016).

19. Splendiani, A., Sun, L., Zhang, Y., Li, T., Kim, J., Chim, C.-Y., Galli, G. & Wang, F. Emerging photoluminescence in monolayer MoS_2. *Nano Lett.* **10**, 1271–1275 (2010).

20. Song, L. et al. Large scale growth and characterization of atomic hexagonal boron nitride layers. *Nano Lett.* **10**, 3209–3215 (2010).

21. Calizo, I., Bejenari, I., Rahman, M., Liu, G. & Balandin, A. A. Ultraviolet Raman microscopy of single and multilayer graphene. *J. Appl. Phys.* **106**, 043509 (2009).

22. Dean, C. R. et al. Boron nitride substrates for high-quality graphene electronics. *Nat. Nanotechnol.* **5**, 722–726 (2010).

23. Kim, K. K., Hsu, A., Jia, X., Kim, S. M., Shi, Y., Dresselhaus, M., Palacios, T. & Kong, J. Synthesis and characterization of hexagonal boron nitride film as a dielectric layer for graphene devices. *ACS Nano* **6**, 8583–8590 (2012).

24. Carvalho, A., Ribeiro, R. M. & Neto, A. H. C. Band nesting and the optical response of two-dimensional semiconducting transition metal dichalcogenides. *Phys. Rev. B* **88**, 115205 (2013).

25. Wang, L. et al. Slow cooling and efficient extraction of C-exciton hot carriers in MoS_2 monolayer. *Nat. Commun.* **8**, 13906 (2017).

26. Mak, K. F., Lee, C., Hone, J. Shan, J. & Heinz, T. F. Atomically thin MoS_2: a new direct-gap semiconductor. *Phys. Rev. Lett.* **105**, 136805 (2010).

27. Buscema, M., Island, J. O., Groenendijk, D. J., Blanter, S. I., Steele, G. A., van der Zant, H. S. J. & Castellanos-Gomez, A. Photocurrent generation with two-dimensional van der Waals semiconductors. *Chem. Soc. Rev.* **44**, 3691–3718 (2015).

28. Fang, H. & Hu, W. Photogating in low dimensional photodetectors. *Adv. Sci.* **4**, 1700323 (2017).

29. Bartolomeo, A. D., Genovese, L., Foller, T., Giubileo, F., Luongo, G., Croin, L, Liang, S.-J., Ang, L. K. & Schleberger, M. Electrical transport and persistent photoconductivity in monolayer MoS_2 phototransistors. *Nanotechnology* **28**, 214002 (2017).

30. Lopez-Sanchez, O., Lembke, D., Kayci, M., Radenovic, A. & Kis, A. Ultrasensitive photodetectors based on monolayer MoS_2. *Nat. Nanotechnol.* **8**, 497–501 (2013).

31. Kufer, D. & Konstantatos, G. Highly sensitive encapsulated MoS_2 photodetector with gate controllable gain and speed. *Nano Lett.* **15**, 7307–7313 (2015).

32. Kozawa, D. et al. Photocarrier relaxation pathway in two-dimensional semiconducting transition metal dichalcogenides. *Nat. Commun.* **5**, 4543 (2014).

33. Shi, H., Yan, R., Bertolazzi, S., Brivio, J., Gao, B., Kis, A., Jena, D., Xing, H. G. & Huang, L. Exciton dynamics in suspended monolayer and few-layer MoS_2 2D crystals. *ACS Nano* **7**, 1072–1080 (2013).

34. Peelaers, H. & Van de Walle, C. G. Effects of strain on band structure and effective masses in MoS_2. *Phys. Rev. B* **86**, 241401(R) (2012).

35. Cheiwchanchamnangij, T. & Lambrecht, W. R. L. Quasiparticle band structure calculation of monolayer, bilayer, and bulk MoS_2. *Phys. Rev. B* **85**, 205302 (2012).

36. Chen, C. et al. Highly responsive MoS_2 photodetectors enhanced by graphene quantum dots. *Sci. Rep.* **5**, 11830 (2015).

37. Wu, Y.-C., Liu, C.-H., Chen, S.-Y., Shih, F.-Y., Ho, P.-H., Chen, C.-W. Liang, C.-T. & Wang, W.-H. Extrinsic origin of persistent photoconductivity in monolayer MoS_2 field effect transistors. *Sci. Rep.* **5**, 11472 (2015).

38. Miyamoto, Y., Yoshikawa, D., Takei, K., Arie, T. & Akita, S. Effect of buffer layer on photoresponse of MoS_2 phototransistor. *Jpn. J. Appl. Phys.* **57**, 06HB01 (2018).

Acknowledgements

The authors appreciate the financial support from the National Creative Research Laboratory program (Grant No. 2012026372) through the National Research Foundation of Korea funded by the Korean Ministry of Science and ICT. S.C. appreciates the support from the Korea Institute of Science and Technology (KIST) Future Resource Research Program (2E29520) and the National Research Foundation of Korea grant (NRF-2017R1C1B2002323)

funded by the Korean Ministry of Science and ICT. W.Y. and I.L. acknowledge the Institute for Basic Science (IBS-R011-D1). G.H.A., and A.J. acknowledge the Electronic Materials Program, funded by the Director, Office of Science, Office of Basic Energy Sciences, Material Sciences and Engineering Division of the U.S. Department of Energy under Contract No. DE-AC02-05CH11231.

Author contributions

T.L. and S.C. supervised the design of experiments and optoelectronic characterization of the transparent MoS_2 phototransistors. J.P. designed and carried out the experiments. I.L. and W.Y. set up the equipment for the optoelectrical experiments and contributed to the measurements. K.C. and K.K. helped to analyze the results of the optoelectronic characterization. H.J. and W.H. grew the CVD monolayer graphene, and J.K. grew the CVD monolayer MoS_2. G.A. and A.J. helped to fabricate transparent van der Waals heterostructures. J.P., S.C. and T.L. contributed to writing and editing the manuscript, and all authors contributed to the data analysis and discussion of the results.

Additional information

Supplementary Information accompanies this paper at http://www.nature.com/naturecommunications

Competing financial interests: The authors declare no competing financial interests.

Reprints and Permission information is available online at http://npg.nature.com/reprintsandpermissions/

How to cite this article Pak J. *et al.* Intrinsic optoelectronic characteristics in MoS_2 phototransistors via a fully transparent van der Waals heterostructure. *Nat. Commun.* ##:#### doi:####

Figure Captions

Figure 1. **| Images, Raman, and PL data for a vdW heterostructure and electrical data for a fully transparent MoS_2 phototransistor.** (**a**) The schematic of the vdW heterostructure on a PEN substrate. (**b**) Optical image of a fabricated fully transparent MoS_2 phototransistor. (**c**) Raman spectra for the CVD-grown monolayer MoS_2 and graphene (denoted as Gr), and mechanically exfoliated multilayer *h*-BN. Scale bar = 5 μm. (**d**) PL mapping image with a 1.86 eV peak intensity. Scale bar = 5 μm. (**e**) I_{DS}-V_{GS} and (**f**) I_{DS}-V_{DS} curves for the fully transparent MoS_2 phototransistor. (**g**) Logarithmic scale plot for I_{DS}-V_{DS} with an average γ value of 1.01.

Figure 2. **| Spectroscopic characteristics of a fully transparent MoS_2 phototransistor.** (**a**) Transmittances (solid lines) and reflectances (dashed lines) corresponding to each heterostructure. (**b**) Absorbance of the CVD-grown monolayer MoS_2 indicating three resonance peaks: A, B, and C. (**c**) Photographic images displaying high transparency.

Figure 3. **| Comparison of the optoelectrical characteristics for MhG and MhS.** The schematics for (**a**) MhG and (**b**) MhS. The thickness for the multilayer *h*-BN was 41 nm and 28 nm for MhG and MhS, respectively. The range of E_{GS} (0.6 MV/cm) corresponds to an applied V_{GS} of 2.46 V and 7.68 V for MhG and MhS, respectively. (**c**-**f**) The photoresponsive characteristics of

MhG and MhS under various illumination conditions with light intensity ranging from 15 nW to 1180 nW at a fixed wavelength of 450 nm, and wavelength ranging from 780 nm to 450 nm at a fixed intensity of 3 μW. (**g**) E_{TH} variation versus illumination intensity and (**h**) the wavelength-dependent responsivity of MhG and MhS at a fixed V_{DS} of 0.5 V and E_{GS} of 0 MV/cm.

Figure 4. **| External and internal optoelectronic characteristics in a fully transparent MoS_2 phototransistor.** (**a**) Contour plots indicating external (upper panel) and internal (lower panel) responsivities as a function of V_{GS} and wavelength at a fixed V_{DS} of 0.5 V and illumination intensity of 3 μW. (**b**) The external and internal responsivities at a fixed wavelength of 600 nm. (**c**) Contour plots comparing EQE (upper panel) and IQE (lower panel) at a fixed V_{DS} of 0.5 V and illumination intensity of 3 μW. The wavelength-dependent (**d**) EQE and (**e**) IQE values (colored circle symbols) corresponding to each V_{GS}. Absorbance for a CVD-grown MoS_2 monolayer is indicated as a red solid line in (**d**).

Figure 5. **| Time-resolved photoresponse characteristics.** (**a**) Photoswitching characteristics of a fully transparent MoS_2 phototransistor under illumination of the MoS_2 channel for 100 s at different V_{DS} conditions of 1.0 V (red open circle symbols) and 0.1 V (blue open circle symbols) at a fixed V_{GS} of –2 V. The solid lines are lines fitted by an exponential decay function. (**b**) τ_1 and τ_2 versus V_{DS} ranging from 0.1 V to 1.0 V. (**c**)

Photoswitching characteristics at different illumination intensities of 1150 nW (red open circle symbols) and 40 nW (blue open circle symbols) at a fixed V_{DS} of 1 V. (**d**) τ_1 and τ_2 versus the illumination intensity ranging from 40 nW to 1150 nW.

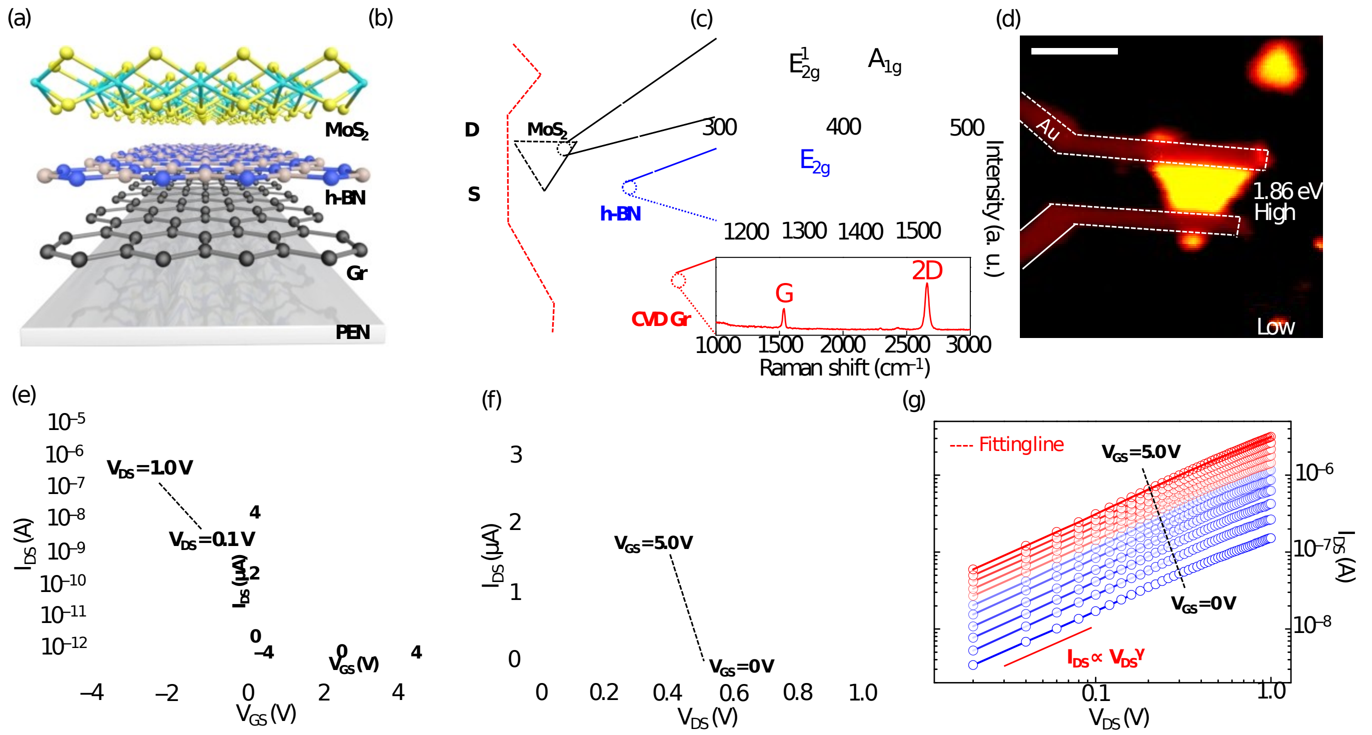

Figure 1. Pak et al.

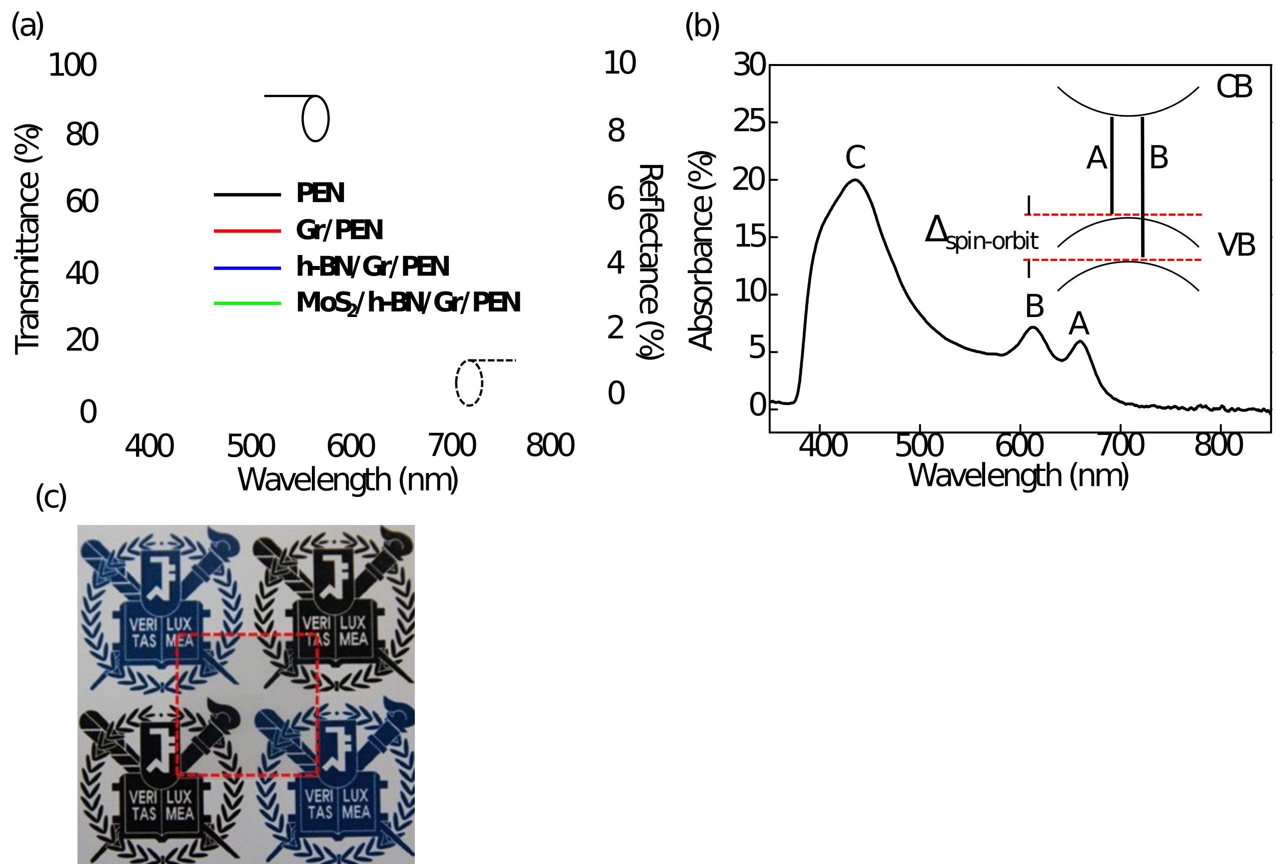

Figure 2. Pak et al.

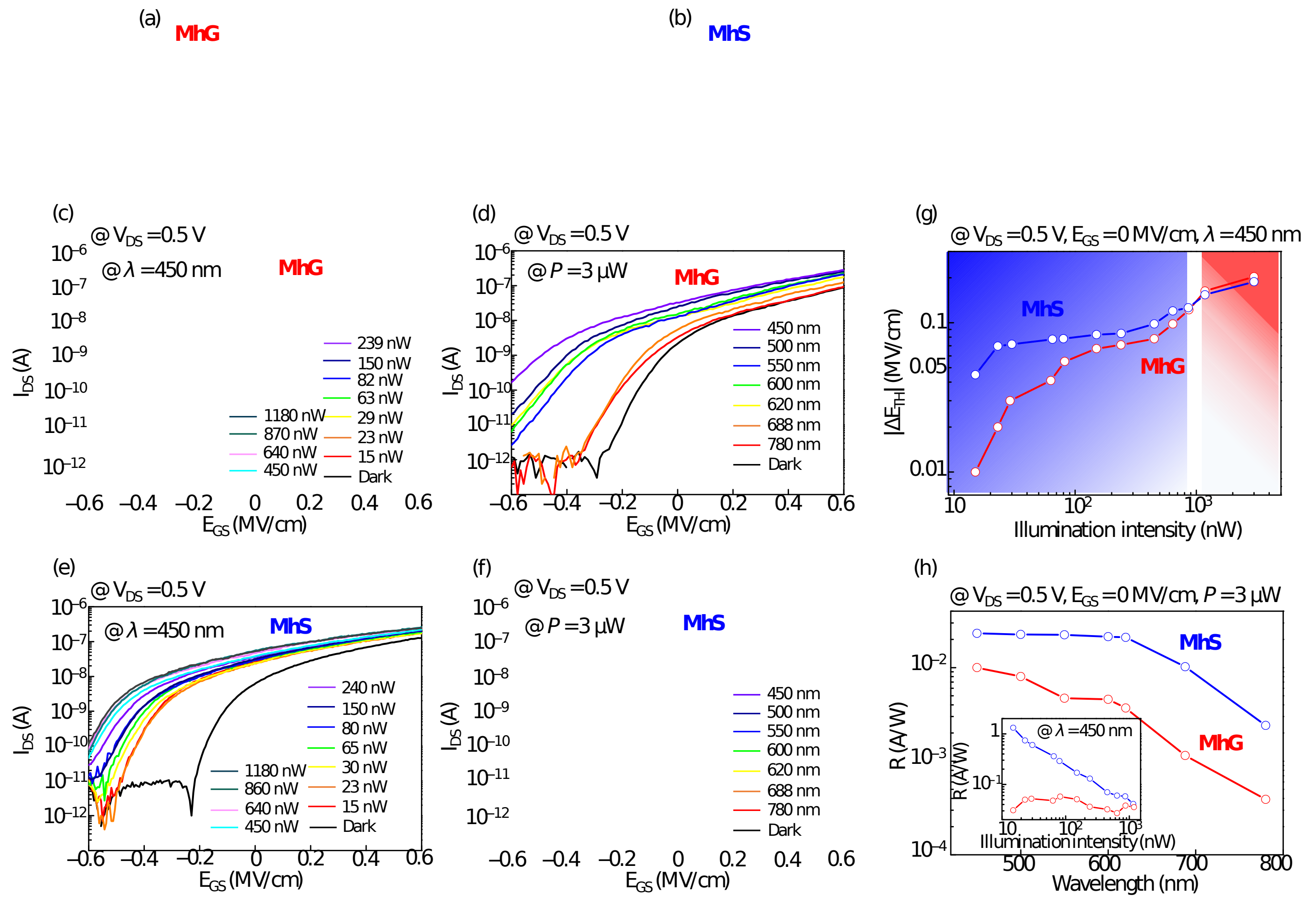

Figure 3. Pak et al.

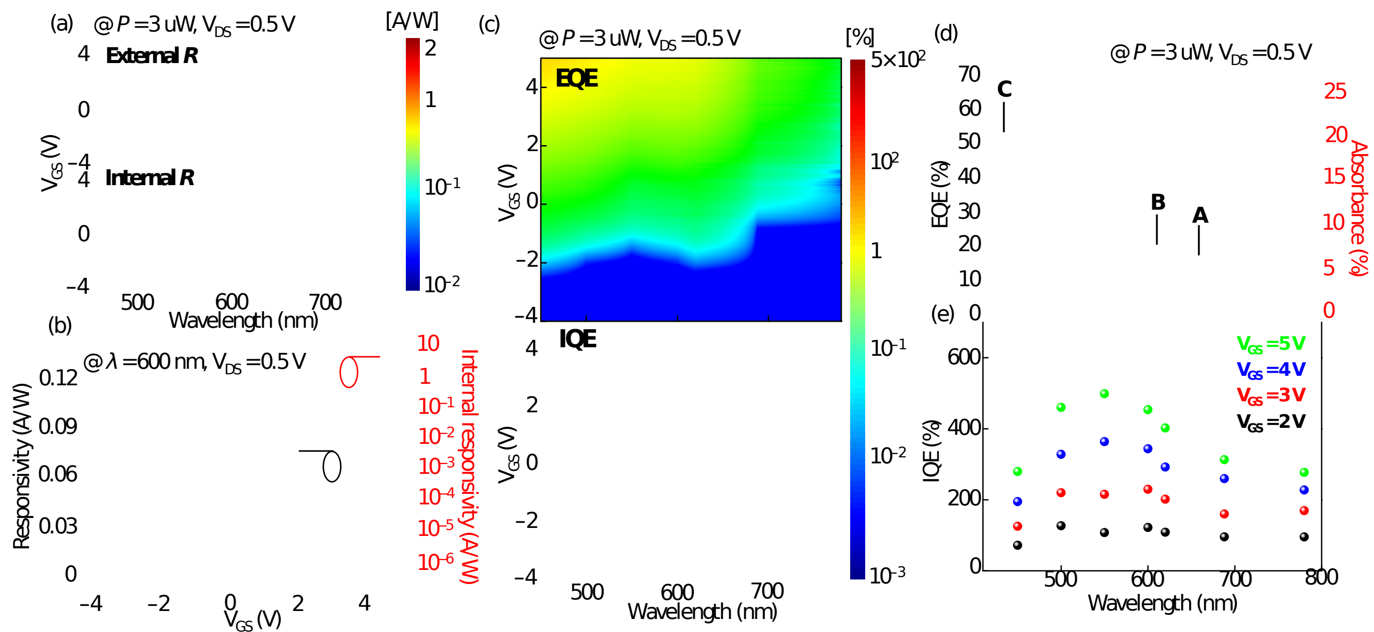

Figure 4. Pak et al.

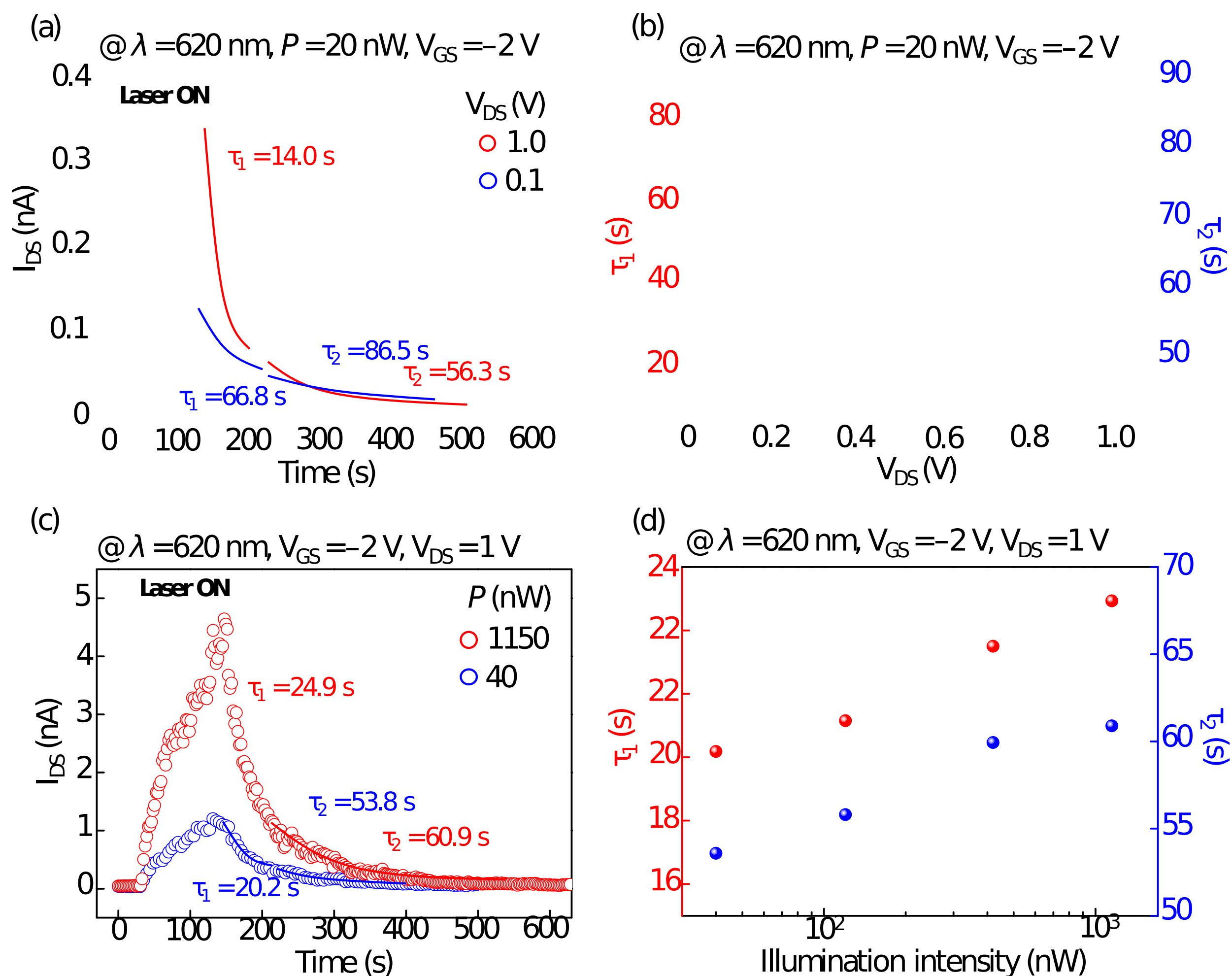

Figure 5. Pak et al.